Tribology International 118 (2018) 140–147

Contents lists available at ScienceDirect

Tribology International

journal homepage: www.elsevier.com/locate/triboint

Discussion on the Reynolds equation for the slipper bearing modeling in axial piston pumps

Qun Chao, Junhui Zhang *, Bing Xu, Qiannan Wang

State Key Laboratory of Fluid Power and Mechatronic Systems, Zhejiang University, China

ARTICLE INFO

Keywords:
Axial piston pump
Slipper bearing
Reynolds equation
Slipper spin

ABSTRACT

This work presents a new Reynolds equation for the slipper bearing in axial piston pumps which considers the slipper spin. As an extension of this new Reynolds equation, some typical cases are derived for different velocity boundary conditions. It is found that the present Reynolds equation is identical in form to that in the previous literature, but they are entirely different from each other in the velocity boundary condition. The reasons for the incorrect velocity boundary condition in the previous studies are analyzed, followed by a calculation of the relative velocity error. It is concluded that the Reynolds equation in the present work is more capable of representing the lubrication model for the slipper bearing.

1. Introduction

Axial piston pumps are widely used in many applications because of their advantages such as high working pressure, great power density, convenient flow regulation, and long service life [1]. A typical axial piston pump is shown in Fig. 1. The cylinder block containing nine pistons rotates together with the shaft by a spline mechanism. The piston connects itself with the slipper through a ball-and-socket joint. All the pistons reciprocate within the cylinder bores and the slippers slide on the inclined swash plate during the cylinder block rotation. A reasonable contact between the slipper and swash plate is maintained using the retainer. The displacement chambers in the cylinder block are communicated with the suction or discharge port by the kidney-shaped ports in the valve plate. When the piston passes over the suction side, it is pulled out of the cylinder bore and the low-pressure fluid flows into the cylinder bore. When the piston passes over the discharge side, it is pushed into the cylinder bore and the high-pressure fluid flows out of the cylinder bore. The above reciprocating motion repeats itself for each revolution of the shaft, accomplishing the basic task of converting the low-pressure fluid into the high-pressure fluid.

The pump performance strongly depends on the lubricating interfaces where the fluid film forms to separate heavily loaded relatively movable parts from each other. There are three main lubricating interfaces within an axial piston pump, the cylinder block/valve plate interface, the piston/cylinder block interface, and the slipper/swash plate interface. These lubricating interfaces serve as sealing and bearing functions, which are one of the critical design issues for axial piston pumps. As for the slipper/swash plate interface, it prevents the pressurized fluid in the displacement chamber from leaking into the pump case through the slipper land. Additionally, the fluid film within it fulfills the function of carrying the pressure load exerted by the piston. Both the sealing and bearing functions of the slipper/swash plate interface are determined by the lubrication characteristics of the slipper bearing, which depend on the slipper's motion on the swash plate. In addition to the macro motion governed by the pump kinematics, the slipper also undergoes some micro motions including tilting motion, squeezing motion, and spinning motion due to the additional degrees of freedom on the micro scale. The performance of the slipper bearing is often represented by its leakage flow, load-carrying capacity, and power losses etc. These critical performance parameters are related to the fluid film thickness and pressure across the slipper bearing which require to be calculated by the Reynolds equation for the slipper bearing.

Iboshi and Yamaguchi [2] derived the Reynolds equation for the slipper bearing from the Navier-Stokes equation to evaluate the fluid film parameters of slipper, including tilting angle, maximum tilting angle azimuth and mean gap height. For mathematical expediency, they simplified the pressure distribution across the slipper bearing as a power series of the slipper's tilting angle. Hooke et al. [3–7] investigated the tilting behavior and lubrication characteristics of the slipper bearing with different slipper running surface profiles theoretically and experimentally. They used the Reynolds equation to solve for the pressure distribution under the slipper land and thus the fluid force and moment

* Corresponding author.
E-mail address: benzjh@zju.edu.cn (J. Zhang).

https://doi.org/10.1016/j.triboint.2017.09.027
Received 12 June 2017; Received in revised form 15 August 2017; Accepted 24 September 2017
Available online 25 September 2017

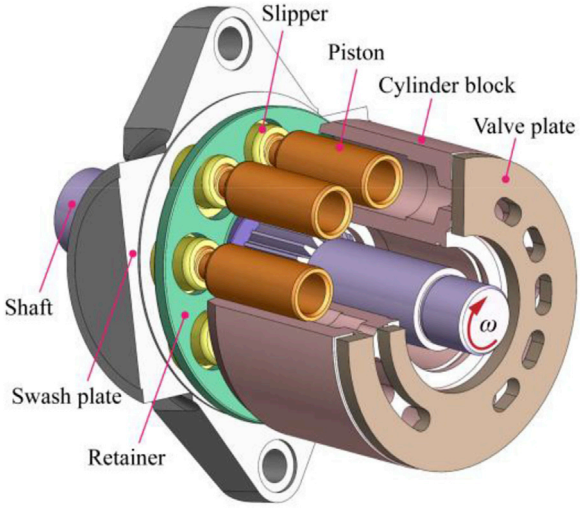

Fig. 1. General configuration of an axial piston pump.

acting on the slipper. The fluid film thickness under the slipper land could be predicted with a reasonable accuracy through solving the force and moment equilibrium equations of the slipper. Wieczorek and Ivantysynova [8,9] performed the pioneering work in the development of the sophisticated simulation tool CASPAR (Calculation of Swash Plate Type Axial Piston Pump/Motor) which was used to simulate the gap flows of the three main lubricating interfaces. As an example, the Reynolds equation for the piston/cylinder block interface was derived from the Navier-Stokes equation and was integrated in the simulation program to determine the gap pressure distribution. However, all the pump components were assumed to be rigid bodies in the simulation program and thus the elastohydrodynamic effects were not considered. Huang [10] extended the CASPAR software and proposed a modified simulation model for the slipper/swash plate interface, which considered the pressure deformation of the slipper and swash plate for the first time. He presented the Reynolds equation for the slipper bearing in cylindrical coordinate systems, in which the velocity on the slipper sliding surface at every grid point was given as the velocity boundary condition. However, we would like to humbly point out that the expression for the velocity on the slipper sliding surface was incorrect due to his misunderstanding of the slipper motion on the swash plate. Specifically, on a macro scale, the slippers do experience curvilinear translation rather than plane rotation on the swash plate. Similarly, Pelosi and Ivantysynova [11] integrated the Reynolds equation into a fluid-structure interaction model inside the simulation tool CASPAR to predict the gap height between the slipper and swash plate. However, they did not provide the velocity boundary condition of the Reynolds equation in detail. Schenk and Ivantysynova [12,13] calculated the power losses generated within the slipper/swash plate interface using the above fully coupled fluid-structure model. Again, the velocity boundary condition of the Reynolds equation was not presented although the same Reynolds equation for the slipper bearing was adopted. Xu et al. [14] conducted numerical and experimental studies on the slipper's partial abrasion phenomenon. In their numerical simulation model for the slipper bearing, they adopted the velocity boundary condition of the Reynolds equation developed by Huang [10]. The slipper spin was not considered in the Reynolds equation for the reason of insufficient theoretical and experimental studies on it. However, in their subsequent work [15] dealing with the effect of case drain pressure on the slipper performance, the slipper spinning speed was included in the Reynolds equation in the modified lubrication model for the slipper bearing. Borghi et al. [16] conducted a numerical study on the dynamic behavior of the slipper bearing, in which the slipper spinning motion was included in the Reynolds equation and its influence on the slipper performance was numerically analyzed. A weakness of this study, however, can be seen in the velocity boundary condition of the Reynolds equation which also failed to describe the slipper motion on the swash plate correctly. Tang et al. [17] developed a mathematical model for the slipper bearing which considered the oil thermal effect to predict the fluid film thickness and temperature within the slipper/swash plate interface under different operating conditions. In their mathematical model they adopted the Reynolds equation for the slipper bearing developed by Borghi et al. [16], therefore their conclusions may remain uncertain. Lin and Hu [18] employed a niche genetic algorithm method to solve their proposed tribo-dynamic model of slipper in which the slipper spinning speed was included in the Reynolds equation. Although the velocity boundary condition of the Reynolds equation was not presented in their paper, it seemed from their Reynolds equation for the slipper bearing that the slipper might also be mistakenly considered to rotate on the swash plate. Unfortunately, Tang et al. [19] used this Reynolds equation for the slipper bearing developed by Lin and Hu [18] in their latest prediction model for the thermoelastohydrodynamic lubrication characteristics of slipper bearing. Bergada et al. [20–22] derived a detailed set of analytical equations for the pressure distribution, leakage flow, and fluid force and moment across the slipper bearing from the Reynolds equation of lubrication. The slipper spinning speed was considered in their analytical model, but further information about how to integrate the slipper spinning speed in the Reynolds equation for the slipper bearing was not provided.

From a thorough review of the literature, it appears that the Reynolds equation for the slipper bearing plays a critical role in predicting the slipper behavior since the performance parameters such as load-carrying capacity, leakage flow, and fluid film thickness require to be calculated by solving it. However, it seems that all the previously mentioned Reynolds equations for the slipper bearing suffer from some serious drawbacks. Firstly, few researchers have derived the Reynolds equation for the slipper bearing in much detail, which leads to an insufficient understanding of it from the physical point of view. Secondly, the velocity boundary condition of the Reynolds equation for the slipper bearing is incorrect in many previous studies. The macro motion of slipper on the swash plate was wrongly considered as plane rotation, but actually the slipper purely translates on the swash plate on a macro scale. Thirdly, many Reynolds equations for the slipper bearing do not take into account the slipper spin for the consideration of insufficient knowledge of the slipper spin. However, the slipper spinning motion does exist within axial piston pumps [23] and has a significant effect on the slipper performance [16]. Therefore, the slipper spin should be included in the Reynolds equations for the slipper bearing.

The goal of this paper is to derive the Reynolds equation for the slipper bearing in cylindrical coordinate systems using the differential analysis of fluid flow. The velocity boundary condition of the Reynolds equation is evaluated based on the slipper kinematics on the swash plate, which accounts for the influence of the slipper spin. Also, the difference of the Reynolds equation for the slipper bearing between this work and previous studies is examined to explain why the new Reynolds equation is more able to represent the slipper bearing lubrication than those in the previous studies.

2. Kinematics of the slipper

To determine the velocity boundary condition of the Reynolds equation for the slipper bearing, an accurate description of the slipper kinematics on the swash plate is required. Fig. 2 shows the schematic of the slipper's macro motion on the swash plate, where two coordinate systems are defined. The (X, Y, Z) system is a global coordinate system which has its origin at the intersection between the centerline of the cylinder block and the special plane passing through all piston head centers. The Y-axis is chosen to be positive in the upward direction and the Z-axis is consistent with the centerline of the cylinder block. The (X_S, Y_S, Z_S) system is defined with respect to the swash plate and shares the

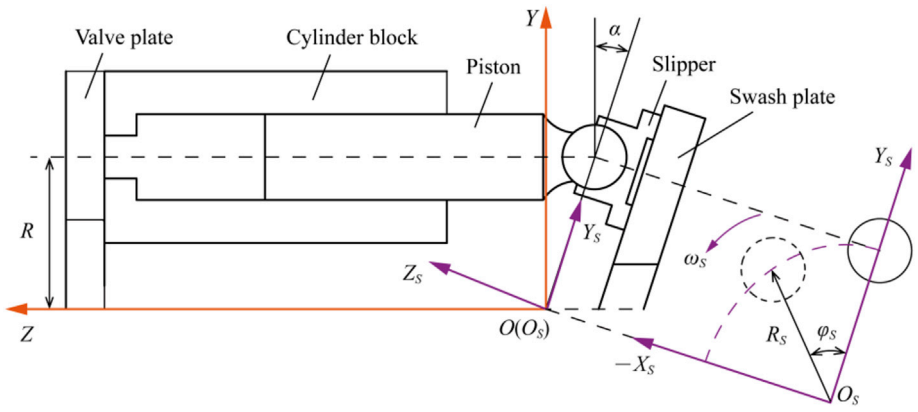

Fig. 2. Schematic of the slipper's macro trajectory on the swash plate.

same origin as the (X, Y, Z) system. The X_SY_S plane is parallel to the swash-plate surface and the Z_S-axis is normal to and pointing away from the swash-plate surface.

The slipper's macro position in the (X, Y, Z) system can be expressed in matrix form as [24].

$$\begin{pmatrix} X \\ Y \\ Z \end{pmatrix} = R \begin{pmatrix} -\sin\varphi \\ \cos\varphi \\ -\tan\alpha\cos\varphi \end{pmatrix} \tag{1}$$

where R is the piston pitch radius, φ is the angular displacement of the slipper in the (X, Y, Z) system, and α is the swash-plate angle.

Pre-multiplying Eq. (1) by the transformation matrix.

$$\mathrm{T} = \begin{pmatrix} 1 & 0 & 0 \\ 0 & \cos\alpha & -\sin\alpha \\ 0 & \sin\alpha & \cos\alpha \end{pmatrix} \tag{2}$$

yields the slipper's macro position on the swash plate described by Eq. (3) in the (X_S, Y_S, Z_S) system.

$$\begin{pmatrix} X_S \\ Y_S \\ Z_S \end{pmatrix} = R \begin{pmatrix} -\sin\varphi \\ \dfrac{1}{\cos\alpha}\cos\varphi \\ 0 \end{pmatrix} \tag{3}$$

It can be seen from Eq. (3) that the slipper's macro trajectory on the swash plate is an elliptical path that can be represented by

$$\frac{X_S^2}{R^2} + \frac{Y_S^2}{(R/\cos\alpha)^2} = 1 \tag{4}$$

whose major axis-length equals $2R/\cos\alpha$ and minor axis-length $2R$.

The position of the slipper on the swash plate can be defined by coordinates (R_S, φ_S).

$$R_S = \sqrt{X_S^2 + Y_S^2} = R\sqrt{1 + \tan^2\alpha\cos^2\varphi} \tag{5}$$

$$\varphi_S = \arctan(-X_S/Y_S) = \arctan(\cos\alpha\tan\varphi) \tag{6}$$

where R_S is the distance of the slipper socket center from the origin of the (X_S, Y_S, Z_S) system, and φ_S is the angular position of the slipper socket center relative to the Y_S-axis.

Assuming the swash-plate is held at a fixed angle, the rotational speed of the slipper socket center about the origin of the (X_S, Y_S, Z_S) system can be obtained by taking the time derivative of Eq. (6).

$$\omega_S = \frac{d\varphi_S}{dt} = \frac{\cos\alpha}{\cos^2\varphi + \cos^2\alpha\sin^2\varphi}\omega \tag{7}$$

where ω is the angular speed of the cylinder block in the (X, Y, Z) system.

It should be pointed out that the slipper purely translates in an elliptical path rather than rotates on the swash plate from the perspective of macro motion. That is to say, at any instant all points on the slipper sliding surface move with the same velocity on the swash plate if the micro motions are not considered. This specific curvilinear translation is illustrated in Fig. 3(a), where an imagined arrow is fixed on the slipper.

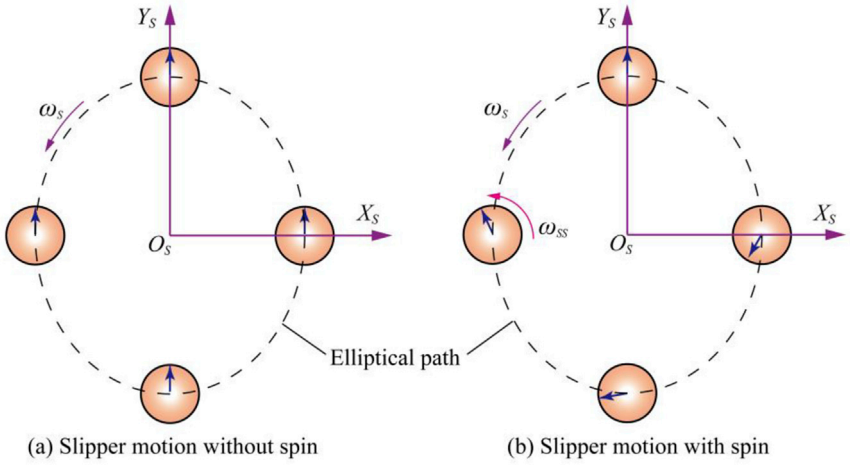

Fig. 3. Comparison of the slippers without and with spinning motion.

Under the assumption of no slipper spin, the direction of the imagined arrow will remain constant even though the slipper translates in an elliptical manner on the swash plate. However, if the slipper has a spinning motion, i.e., rotates about its own axis, the imagined arrow will change its direction, as shown in Fig. 3(b). The time rate of change in the direction of the imagined arrow is determined by the slipper spinning speed ω_{SS}. Therefore, if the spinning motion occurs, the slipper will have an additional angular speed on the swash plate besides a macroscopic translational velocity.

To obtain the velocity boundary condition of the Reynolds equation for the slipper bearing, the velocity on the slipper land surface needs to be calculated for both slippers without and with spinning motion. As shown in Fig. 4, a local coordinate system (x_S, y_S, z_S) is defined using a reference slipper body. The origin of the (x_S, y_S, z_S) system is located at the center of the circular slipper land and lies in the elliptical path defined by Eq. (4). The positive x_S-axis remains tangential to the trajectory of the slipper's slipper land center, while positive y_S-axis is directed radially outwards. The z_S-axis is normal to the slipper land and points away from the slipper socket according to the right-hand rule. An equivalent cylindrical coordinate system (r, θ, z_S) is also introduced, which shares a common origin and z_S-axis with the (x_S, y_S, z_S) system. In the cylindrical coordinate system, θ is measured from the y_S-axis and the counterclockwise rotation is supposed to be positive.

When the slipper slides on the swash plate without the spinning motion, as shown in Fig. 4(a), all points on the slipper sliding surface have the same translational velocity which can be expressed as

$$v_T = \omega_S R_S = \frac{\cos\alpha\sqrt{1+\tan^2\alpha\cos^2\varphi}}{\cos^2\varphi+\cos^2\alpha\sin^2\varphi}\omega R \tag{8}$$

The above translational velocity can be divided into two components in the radial and tangential directions.

$$v_{Tr} = v_T\sin\theta = \frac{\cos\alpha\sqrt{1+\tan^2\alpha\cos^2\varphi}}{\cos^2\varphi+\cos^2\alpha\sin^2\varphi}\omega R\sin\theta \tag{9}$$

$$v_{T\theta} = v_T\cos\theta = \frac{\cos\alpha\sqrt{1+\tan^2\alpha\cos^2\varphi}}{\cos^2\varphi+\cos^2\alpha\sin^2\varphi}\omega R\cos\theta \tag{10}$$

If the slipper translates with spinning motion on the swash plate, as shown in Fig. 4(b), then an additional tangential velocity $v_{S\theta}$ associated with the spinning motion will be generated. The resulting tangential velocity is given by

$$v_{TS\theta} = v_{T\theta} + v_{S\theta} = v_{T\theta} + \omega_{SS} r \tag{11}$$

3. Differential analysis of fluid flow

Fig. 5(a) shows the fluid film under the slipper land. Note that the

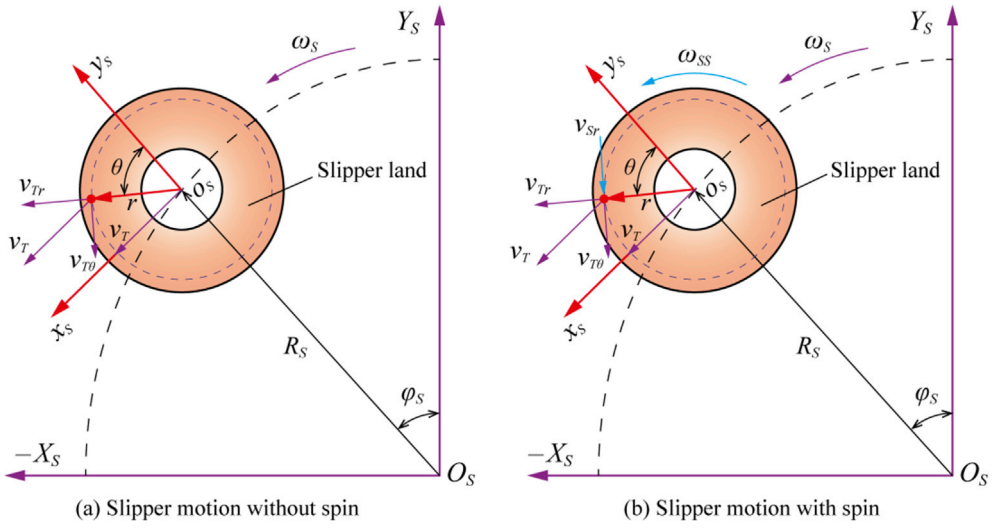

(a) Slipper motion without spin (b) Slipper motion with spin

Fig. 4. Comparison of the velocities on the slipper land without and with spinning motion.

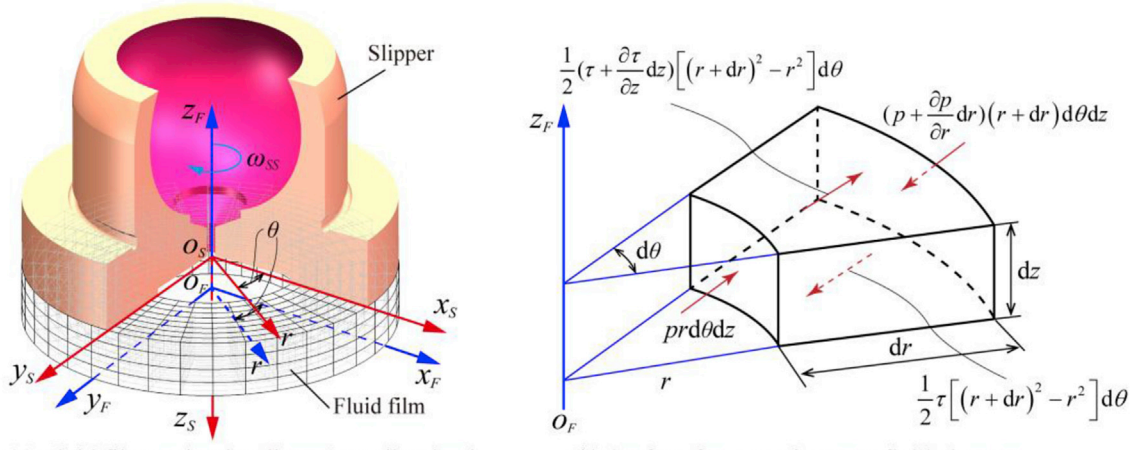

(a) Fluid film under the slipper's sealing land (b) Surface forces acting on a fluid element

Fig. 5. Surface forces acting on a fluid element.

fluid film thickness between the slipper and swash plate is exaggerated for illustration purpose. Actually, the fluid film thickness is on the order of microns for a typical slipper/swash plate interface. Besides the local coordinate system (x_S, y_S, z_S) associated with the slipper, another local coordinate system (x_F, y_F, z_F) associated with the fluid film is defined, whose origin lies in the swash plate plane and is located at the center of the boundary surface of the circular fluid film. The x_F-axis and y_F-axis are parallel to the x_S-axis and y_S-axis, respectively, while the z_F-axis is in the opposite direction to the z_S-axis. Similarly, an equivalent cylindrical coordinate system (r, θ, z_F) is also defined, whose origin coincides with that of the (x_F, y_F, z_F) system. Fig. 5(b) illustrates a fluid element from the fluid film under the slipper land. For simplicity, only the surface forces in the radial direction acting on the fluid element has been illustrated in Fig. 5(b), but, in practice, there are also surface forces along the circumferential direction. Before deriving the Reynolds equation for the slipper bearing in terms of cylindrical coordinate systems, the following assumptions regarding the fluid behavior within the slipper/swash plate lubricating interface are imposed [10,12,13]:

(a) Fluid flow within the slipper bearing is steady and incompressible.
(b) Pressure in the gap height direction is considered constant.
(c) Inertial forces of the fluid are small when compared to the viscous forces, and thus can be neglected.
(d) Body forces of the fluid are negligible.

Considering these assumptions, summing all the surface forces in the radial direction yields the equilibrium equation for the fluid element in the radial direction.

$$p r\mathrm{d}\theta\mathrm{d}z + \frac{1}{2}\left(\tau + \frac{\partial \tau}{\partial z}\mathrm{d}z\right)\left[(r+\mathrm{d}r)^2 - r^2\right]\mathrm{d}\theta = \left(p + \frac{\partial p}{\partial r}\mathrm{d}r\right)(r+\mathrm{d}r)\mathrm{d}\theta\mathrm{d}z + \frac{1}{2}\tau\left[(r+\mathrm{d}r)^2 - r^2\right]\mathrm{d}\theta \tag{12}$$

where τ is the shearing stress, and p is the pressure acting on the fluid element. With $\tau = \mu\frac{\partial v_{or}}{\partial z}$, $\mathrm{d}r \ll r$, and $\mathrm{d}z \ll r$, Eq. (12) can be rearranged to

$$\mu\frac{\partial^2 v_{or}}{\partial z^2} = \frac{\partial p}{\partial r} \tag{13}$$

where μ is the dynamic viscosity of the fluid, and v_{or} is the fluid velocity in the radial direction.

Similarly, the equilibrium equation for the fluid element in the tangential direction is given by

$$\mu\frac{\partial^2 v_{o\theta}}{\partial z^2} = \frac{1}{r}\frac{\partial p}{\partial \theta} \tag{14}$$

where $v_{o\theta}$ is the fluid velocity in the tangential direction.

Integrating Eq. (13) twice over the fluid film thickness yields the expression for the fluid velocity v_{or}.

$$v_{or} = \frac{1}{\mu}\left(\frac{1}{2}\frac{\partial p}{\partial r}z^2 + c_1 z + c_2\right) \tag{15}$$

where the two constants c_1 and c_2 can be determined from the velocity boundary conditions: $v_{or} = 0$ for $z = 0$, and $v_{or} = v_{Tr}$ for $z = h$. Thus, the fluid velocity in the radial direction becomes

$$v_{or} = \frac{1}{2\mu}\frac{\partial p}{\partial r}\left(z^2 - hz\right) + v_{Tr}\frac{z}{h} \tag{16}$$

Similarly, considering the velocity boundary conditions: $v_{o\theta} = 0$ for $z = 0$, and $v_{o\theta} = v_{T\theta} + \omega_{SS}r$ for $z = h$, the tangential fluid velocity with the slipper spin is

$$v_{o\theta} = \frac{1}{2\mu r}\frac{\partial p}{\partial \theta}\left(z^2 - hz\right) + \left(v_{T\theta} + \omega_{SS}r\right)\frac{z}{h} \tag{17}$$

For steady, incompressible flow, the continuity equation in cylindrical coordinate systems can be expressed as

$$\frac{1}{r}\frac{\partial (r v_{or})}{\partial r} + \frac{1}{r}\frac{\partial v_{o\theta}}{\partial \theta} + \frac{\partial v_{oz}}{\partial z} = 0 \tag{18}$$

where v_{oz} is the fluid velocity in the fluid film thickness direction.

Substituting Eqs. (16) and (17) into Eq. (18), and then integrating Eq. (18) over the fluid film thickness yields the Reynolds equation for the slipper bearing with the spinning motion in cylindrical coordinate systems.

$$\frac{1}{r}\frac{\partial}{\partial r}\left(\frac{rh^3}{\mu}\frac{\partial p}{\partial r}\right) + \frac{1}{r^2}\frac{\partial}{\partial \theta}\left(\frac{h^3}{\mu}\frac{\partial p}{\partial \theta}\right) = 6\frac{1}{r}\frac{\partial}{\partial r}(r v_{Tr}h) + 6\frac{1}{r}\frac{\partial}{\partial \theta}\left[(v_{T\theta} + \omega_{SS}r)h\right] + 12\left(v_{oz}|_{z=h} - v_{oz}|_{z=0}\right) \tag{19}$$

Recognizing that $v_{oz}|_{z=h} - v_{oz}|_{z=0} = \frac{\partial h}{\partial t}$, Eq. (19) can be reduced to

$$\frac{1}{r}\frac{\partial}{\partial r}\left(\frac{rh^3}{\mu}\frac{\partial p}{\partial r}\right) + \frac{1}{r^2}\frac{\partial}{\partial \theta}\left(\frac{h^3}{\mu}\frac{\partial p}{\partial \theta}\right) = 6\frac{1}{r}\frac{\partial}{\partial r}(r v_{Tr}h) + 6\frac{1}{r}\frac{\partial}{\partial \theta}\left[(v_{T\theta} + \omega_{SS}r)h\right] + 12\frac{\partial h}{\partial t} \tag{20}$$

Considering $\frac{1}{r}\frac{\partial}{\partial r}(r v_{Tr}h) = \frac{v_{Tr}h}{r} + \frac{\partial}{\partial r}(v_{Tr}h)$ and $\frac{1}{r}\frac{\partial}{\partial \theta}\left[(v_{T\theta} + \omega_{SS}r)h\right] = \frac{h}{r}\frac{\partial v_{T\theta}}{\partial \theta} + \frac{v_{T\theta}}{r}\frac{\partial h}{\partial \theta} + \omega_{SS}\frac{\partial h}{\partial \theta}$ with $h \ll r$, Eq. (20) can be reduced to

$$\frac{1}{r}\frac{\partial}{\partial r}\left(\frac{rh^3}{\mu}\frac{\partial p}{\partial r}\right) + \frac{1}{r^2}\frac{\partial}{\partial \theta}\left(\frac{h^3}{\mu}\frac{\partial p}{\partial \theta}\right) = 6\frac{\partial}{\partial r}(v_{Tr}h) + 6\left(\frac{v_{T\theta}}{r} + \omega_{SS}\right)\frac{\partial h}{\partial \theta} + 12\frac{\partial h}{\partial t} \tag{21}$$

On the other hand, the term $\frac{\partial}{\partial r}(v_{Tr}h)$ in Eq. (21) is equivalent to $v_{Tr}\frac{\partial h}{\partial r}$ since the radial velocity v_{Tr} is independent of the variable r, as presented in Eq. (9). Thus, the final expression of the Reynolds equation for the slipper bearing with the spinning motion becomes

$$\frac{1}{r}\frac{\partial}{\partial r}\left(\frac{rh^3}{\mu}\frac{\partial p}{\partial r}\right) + \frac{1}{r^2}\frac{\partial}{\partial \theta}\left(\frac{h^3}{\mu}\frac{\partial p}{\partial \theta}\right) = 6v_{Tr}\frac{\partial h}{\partial r} + 6\left(\frac{v_{T\theta}}{r} + \omega_{SS}\right)\frac{\partial h}{\partial \theta} + 12\frac{\partial h}{\partial t} \tag{22}$$

The first two terms on the right-hand side of the Reynolds equation stand for the hydrodynamic effect caused by the slipper's translational motion and spinning motion. It can be seen that the slipper spinning motion affects the hydrodynamic effect in relation with the tangential velocity component. The third term on the right-hand side represents the squeezing effect caused by the slipper's micro shifting motion with respect to the swash plate.

If the slipper has no spinning motion, but has translational motion, then $\omega_{SS} = 0$ and Eq. (22) can be reduced to

$$\frac{1}{r}\frac{\partial}{\partial r}\left(\frac{rh^3}{\mu}\frac{\partial p}{\partial r}\right) + \frac{1}{r^2}\frac{\partial}{\partial \theta}\left(\frac{h^3}{\mu}\frac{\partial p}{\partial \theta}\right) = 6v_{Tr}\frac{\partial h}{\partial r} + 6\frac{v_{T\theta}}{r}\frac{\partial h}{\partial \theta} + 12\frac{\partial h}{\partial t} \tag{23}$$

If the slipper has no translational motion, but has spinning motion, then $v_{Tr} = v_{T\theta} = 0$ and Eq. (22) can be reduced to

$$\frac{1}{r}\frac{\partial}{\partial r}\left(\frac{rh^3}{\mu}\frac{\partial p}{\partial r}\right) + \frac{1}{r^2}\frac{\partial}{\partial \theta}\left(\frac{h^3}{\mu}\frac{\partial p}{\partial \theta}\right) = 6\omega_{SS}\frac{\partial h}{\partial \theta} + 12\frac{\partial h}{\partial t} \tag{24}$$

Furthermore, if the slipper has neither spinning motion and translational motion, then $\omega_{SS} = v_{Tr} = v_{T\theta} = 0$ and Eq. (22) can be further simplified as

$$\frac{1}{r}\frac{\partial}{\partial r}\left(\frac{rh^3}{\mu}\frac{\partial p}{\partial r}\right)+\frac{1}{r^2}\frac{\partial}{\partial \theta}\left(\frac{h^3}{\mu}\frac{\partial p}{\partial \theta}\right)=12\frac{\partial h}{\partial t} \tag{25}$$

4. Comparison of Reynolds equation for the slipper bearing

Taking the slipper bearing without spinning motion for example, this section will present the comparison of Reynolds equation for the slipper bearing between this work and previous studies. Although the Reynolds equation for the slipper bearing in this work has almost the same form as that in the previous literature [10–19], it cannot be taken for granted that they are identical to each other from the physical point of view. There is a marked difference in the velocity boundary condition of the Reynolds equation between this work and previous studies. The previous studies often failed to evaluate the velocity boundary condition of the Reynolds equation correctly. The previous calculation of the boundary velocity for the slipper bearing could be mainly divided into two types.

First, the slipper was considered to slide in a circular path instead of an elliptical one, as shown in Fig. 6(a). As a result, the distance R_S of the slipper socket center from the origin of the (X_S, Y_S, Z_S) system remained equal to the piston pitch radius R [16–19]. Alternatively, the rotational speed ω_S of the slipper socket center about the origin of the (X_S, Y_S, Z_S) system was supposed to be the same as the angular speed ω of the cylinder block [10,16–19]. However, it can be seen from Eqs. (5) and (7) that the above approximations are practically impossible unless the swash-plate angle α equals zero.

Second, the previous studies [10,14–19] failed to correctly describe the slipper's macro motion on the swash plate. Specifically, the slipper motion on the swash plate was supposed to be subjected to plane rotation rather than curvilinear translation. The assumption of the plane rotation for the slipper would lead to a non-uniform velocity distribution on the slipper face, as shown in Fig. 6(b). In other words, the velocity on the slipper face in each grid point (r, θ) was expressed as

$$v_T=\omega_S R_M=\omega_S\sqrt{r^2+R_S^2+2rR_S\cos\theta} \tag{26}$$

Eq. (26) suggests that the translational velocity v_T of the slipper on the swash plate is dependent on the radial coordinate r in the local cylindrical coordinate system (r, θ, z_S). However, in practice, the translational velocity v_T is independent of the radial coordinate r due to the curvilinear translation of the slipper, as presented in Eq. (8).

5. Discussion

It is clear that neither the assumption of the slipper's macro motion in circular path nor of its plane rotation on the swash plate is practically possible. Furthermore, if the slipper undergoes a plane rotation rather than translation on the swash plate, then the velocity v_T on the slipper face is dependent on the radial coordinate r, as presented in Eq. (26). This means that the term $\frac{\partial}{\partial r}(v_{Tr}h)$is no longer equivalent to $v_{Tr}\frac{\partial h}{\partial r}$, and the Reynolds equation for the slipper bearing in the previous studies is impossible to be the same in form as that in Eq. (23). Therefore, the Reynolds equation for the slipper bearing in the previous studies is in conflict with the assumption of the slipper's plane rotation on the swash plate.

It is a meaningful attempt to investigate the effect of the previous assumption of the slipper's plane rotation on the boundary velocity for the slipper bearing. Making use of the Taylor series expansion, the velocity on the slipper face in Eq. (26) can be rewritten as

$$v_T=\omega_S R_S\left[1+\frac{1}{2}\xi-\frac{1}{8}\xi^2+R_2(\xi)\right] \tag{27}$$

where $R_2(\xi)$ is the remainder term of the Taylor's formula, and ξ is given by

$$\xi=\frac{r^2+2rR_S\cos\theta}{R_S^2} \tag{28}$$

Then the velocity error due to the previous assumption of the slipper's plane rotation can be expressed as

$$\Delta v_T=\omega_S R_S\left[\frac{1}{2}\xi-\frac{1}{8}\xi^2+R_2(\xi)\right] \tag{29}$$

And the relative velocity error is defined as

$$\Delta_R=\frac{\Delta v_T}{\omega_S R_S}=\frac{1}{2}\xi-\frac{1}{8}\xi^2+R_2(\xi) \tag{30}$$

Recognizing that ξ is much less than unity for the slipper bearing, the higher-order terms of ξ in Eq. (30) can be neglected. Thus, for small ξ, the relative velocity error may be approximately equal to

$$\Delta_R=\frac{1}{2}\xi \tag{31}$$

This equation shows that the relative velocity error Δ_R depends on the angular positions of the slipper both in the X_SY_S plane and the $r\theta$ plane, and the geometrical features of axial piston machines, including piston pitch radius, internal and external radii of the slipper land, and swash-

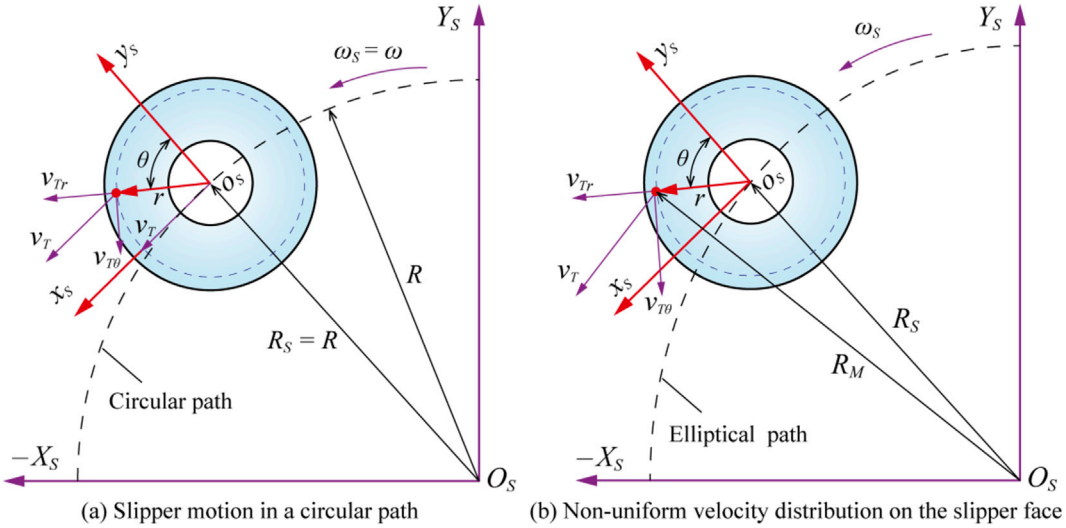

Fig. 6. Boundary velocity for the slipper bearing in the previous studies.

plate angle. Table 1 lists the above geometrical features of a typical commercial axial piston pump.

Fig. 7 shows the distribution of the relative velocity error on the slipper land when the slipper slides on the swash plate. It can be observed that the effect of the previous assumption of the slipper's plane rotation on the relative velocity error mainly depends on the location (r, θ) of each grid point in the local cylindrical coordinate system. For each angular position of the slipper, the relative velocity error is positive for $-90^\circ \leq \theta \leq 90^\circ$, but negative for $90^\circ \leq \theta \leq 270^\circ$. The large absolute relative velocity errors occur at the outer region of $-45^\circ \leq \theta \leq 45^\circ$ and $135^\circ \leq \theta \leq 225^\circ$ on the slipper land. This can be explained by the fact that the velocity on the slipper face within these two areas is most likely to be overestimated or underestimated according to Eq. (31). When the slipper is located at the minor axis of the elliptical path, the relative velocity error reaches the maximum of 0.37 at the intersection between the external edge of the slipper land (i.e., $r = R_o$) and the positive y_S-axis (i.e., $\theta = 0$). The minimum relative velocity error of −0.27 also takes place at the minor axis of the elliptical path, but its corresponding position is determined by the external edge of the slipper land and the negative y_S-axis (i.e., $\theta = 180^\circ$). In addition, the distribution of the relative velocity error is almost symmetric about the y_S-axis, this is because Eq. (31) becomes a cosine function of θ after neglecting the higher-order term of r/R_S, i.e., $(r/R_S)^2$.

Table 1
Geometrical features of a typical commercial axial piston pump.

Description	Value	Description	Value
Displacement V_g	71 mL/r	Internal radius of the slipper land R_i	6.55 mm
Maximum swash-plate angle α	17.2 deg	External radius of the slipper land R_o	12.95 mm
Piston pitch radius R	40.5 mm		

6. Conclusions

The Reynolds equation is essential for the prediction of the slipper's dynamic behavior. In this work, the Reynolds equation for the slipper bearing is derived from the equilibrium equation and continuity equation, and its velocity boundary condition is clarified for the first time. Also, the comparison of the Reynolds equation for the slipper bearing is presented in detail between the present work and previous studies. Based on the analytical results, the following conclusions may be drawn:

(1) The present Reynolds equation for the slipper bearing without the spinning motion (see Eq. (23)) is identical in form to that in the previous studies, but they are different from each other in the velocity boundary condition.
(2) For the slipper bearing, the velocity boundary condition for the Reynolds equation is determined by the slipper's macro motion and spinning motion on the swash plate. The slipper does experience a translation in an elliptical manner rather than a plane rotation on the swash plate.
(3) The assumption of the slipper's plane rotation on the swash plate in the previous studies will cause a significant relative error of up to 0.37 for the boundary velocity of the slipper bearing in a commercial axial piston machine.
(4) The Reynolds equation for the slipper bearing with the spinning motion is derived in this work (see Eq. (22)). It is found that the spinning speed of the slipper only influences the hydrodynamic

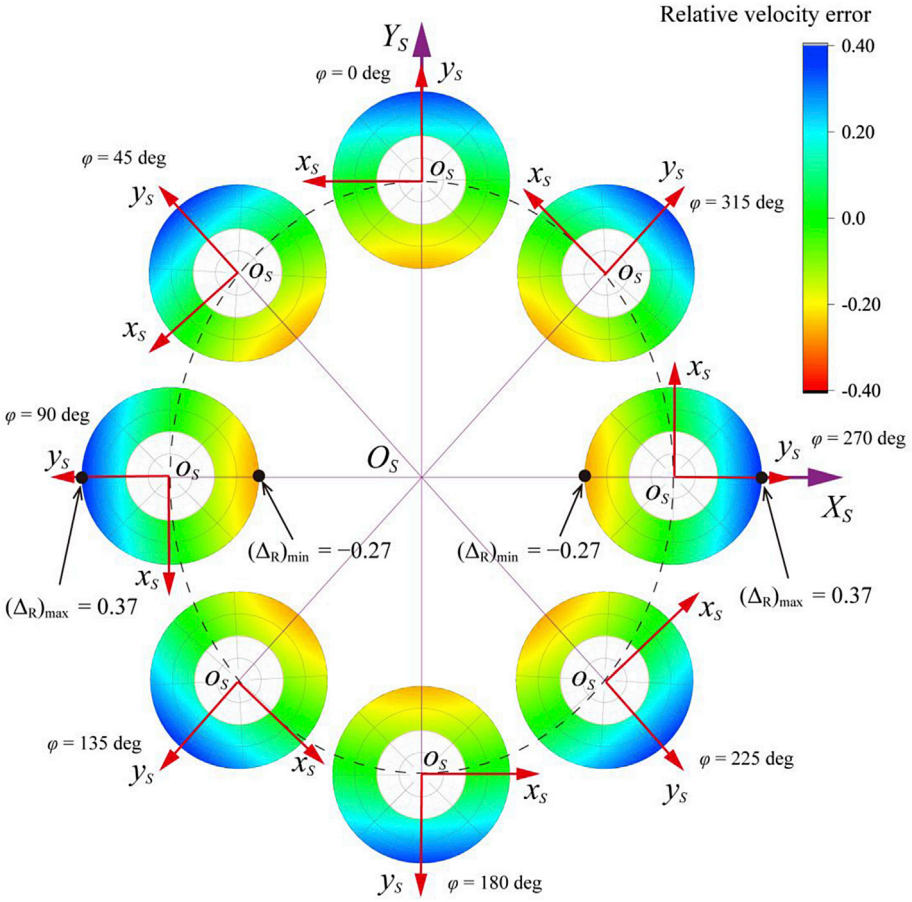

Fig. 7. Distribution of the relative velocity error for the slipper bearing without spinning motion.

effect associated with the tangential velocity component in the Reynolds equation.

Acknowledgements

The authors gratefully acknowledge the financial support from National Basic Research Program of China (973 Program) (No. 2014CB046403) and National Natural Science Foundation of China (No. U1509204).

References

[1] Yang HY, Pan M. Engineering research in fluid power: a review. J Zhejiang Univ-SCI A 2015;16(6):427–42.
[2] Iboshi N, Yamaguchi A. Characteristics of a slipper bearing for swash plate type axial piston pumps and motors: 1st report, theoretical analysis. Bull JSME 1982; 25(210):1921–30.
[3] Hooke CJ, Kakoullis YP. The effects of non-flatness on the performance of slippers in axial piston pumps. Proc Inst Mech Eng Part C J Eng Mech Eng Sci 1983;197(4): 239–47.
[4] Hooke CJ, Li KY. The lubrication of overclamped slippers in axial piston pumps—centrally loaded behaviour. Proc Inst Mech Eng Part C J Eng Mech Eng Sci 1988;202(4):287–93.
[5] Hooke CJ, Li KY. The lubrication of slippers in axial piston pumps and motors—the effect of tilting couples. Proc Inst Mech Eng Part C J Eng Mech Eng Sci 1989;203(5): 343–50.
[6] Koc E, Hooke CJ. Investigation into the effects of orifice size, offset and overclamp ratio on the lubrication of slipper bearings. Tribol Int 1996;29(4):299–305.
[7] Koc E, Hooke CJ. Considerations in the design of partially hydrostatic slipper bearings. Tribol Int 1997;30(11):815–23.
[8] Wieczorek U, Ivantysynova M. CASPAR-a computer-aided design tool for axial piston machines. In: Bath workshop on power transmission and motion control. UK: University of Bath; 2000. p. 113–26.
[9] Wieczorek U, Ivantysynova M. Computer aided optimization of bearing and sealing gaps in hydrostatic machines—the simulation tool CASPAR. Int J Fluid Power 2002; 3(1):7–20.
[10] Huang CC. CASPAR based slipper performance prediction in axial piston pumps. In: Proceeding of the 3rd FPNI-PhD symposium on fluid power. Spain; 2004. p. 229–38.
[11] Pelosi M, Ivantysynova M. A new fluid structure interaction model for the slipper-swashplate interface. In: Proceeding of the 5th FPNI PhD symposium. Poland; 2008. p. 219–36.
[12] Schenk A, Ivantysynova M. An investigation of the impact of elastohydrodynamic deformation on power loss in the slipper swashplate interface. In: 8th JFPS international symposium on fluid power. Japan; 2011.
[13] Schenk A, Ivantysynova M. Design and optimization of the slipper-swashplate interface using an advanced fluid structure interaction model. In: Proceedings of the 52nd national conference on fluid power. USA; 2011. p. 91–100.
[14] Xu B, Zhang JH, Yang HY. Investigation on structural optimization of anti-overturning slipper of axial piston pump. Sci China-Technol Sci 2012;55(11):3010–8.
[15] Xu B, Wang QN, Zhang JH. Effect of case drain pressure on slipper/swashplate pair within axial piston pump. J Zhejiang Univ-SCI A 2015;16(12):1001–14.
[16] Borghi M, Specchia E, Zardin B. Numerical analysis of the dynamic behaviour of axial piston pumps and motors slipper bearings. SAE Int J Passeng Cars-Mech Syst 2009;2(2009–01-1820):1285–302.
[17] Tang HS, Yin YB, Li J. Lubrication characteristics analysis of slipper bearing in axial piston pump considering thermal effect. Lubr Sci 2016;28(2):107–24.
[18] Lin S, Hu J. Tribo-dynamic model of slipper bearings. Appl Math Model 2015;39(2): 548–58.
[19] Tang HS, Ren Y, Xiang JW. A novel model for predicting thermoelastohydrodynamic lubrication characteristics of slipper pair in axial piston pump. Int J Mech Sci 2017;124:109–21.
[20] Bergada JM, Watton J. Force and flow through hydrostatic slippers with grooves. In: 8th international symposium on fluid control measurement and visualization. China; 2005.
[21] Bergada JM, Haynes JM, Watton J. Leakage and groove pressure of an axial piston pump slipper with multiple lands. Tribol Trans 2008;51(4):469–82.
[22] Bergada JM, Kumar S, Davies DL, Watton J. A complete analysis of axial piston pump leakage and output flow ripples. Appl Math Model 2012;36(4):1731–51.
[23] Zhang JH, Chao Q, Wang QN, Xu B, Chen Y, Li Y. Experimental investigations of the slipper spin in an axial piston pump. Measurement 2017;102:112–20.
[24] Hashemi S, Kroker A, Bobach L, Bartel D. Multibody dynamics of pivot slipper pad thrust bearing in axial piston machines incorporating thermal elastohydrodynamics and mixed lubrication model. Tribol Int 2016;96:57–76.